A Novel Parallel-Excited Dual-PM Reluctance Machine with Enhanced Torque and Efficiency Performance

Jifu Jiang, Shuangxia Niu, *IEEE Senior Member* and Xing Zhao

***Abstract*—This paper presents a novel parallel-excited dual-PM reluctance machine (DPM-RM) with enhanced torque and efficiency performance. The key is to build an integrated magnetic field with two sets of PM excitation sources in both stator yoke and slot openings. Two excitation sources produce a parallel magnetic field, which contributes to a superimposed magnetic flux in the airgap, thus leading to strengthened flux variation, improved back-EMF and torque. Additionally, with a special slot/pole combination, biased component and even order harmonics in the phase magnetic flux are eliminated to make the phase flux linkage more sinusoidal. In the meantime, self-inductance variation is greatly suppressed with odd order harmonics of self-inductance removed, resulting in suppressed torque ripple. The prototype is manufactured, and experiments are carried out to verify the effectiveness of the machine design.**

***Index Terms*—Parallel excitation, reluctance motor, slot-PM, torque ripple.**

I. Introduction

VARIABLE reluctance machines (VRMs) whose rotor consist of only iron core , have the merits of simple machine structure, mechanical robustness, less maintenance, as well as relatively low manufacturing cost [1-2]. According to excitation source difference, VRMs can be classified into no-independent excitation VRMs, DC-excited VRMs, and PM-excited VRMs. No-independent excitation VRMs include switched reluctance machines (SRMs), stepper machines, and synchronous reluctance machines [3-4]. For DC-excited VRMs, the efficiency is limited since the excitation loss is needed to be considered [5]. For PM-excited VRMs, PMs can be placed in the stator or rotor. Even through PMs mounting in the rotor will enhance the torque density, it will also lead to mechanical instability and thermal problem [6]. Therefore, PMs are placed in the stator, and doubly salient PM machine (DSPMM) is formed in this way [7]. The conventional DSPMM, which is one kind of PM-excited VRMs, incorporates the merits of both salient pole rotor and stator PM excitation, which includes: 1) simple structure and mechanical robustness with salient pole rotor. 2) less maintenance and manufacturing cost. 3) high torque density and power density. 4) high efficiency comparing with no excitation and DC-excited VRMs. 5) easy to heat dissipation since all sources located in the stator. The 3-phase 6/4 pole configuration with the simplest structure is the first DSPMM being proposed [8]. Two PMs are placing in the stator to provide excitation flux. In order to attain higher power density, wider speed range, lower torque ripple and higher efficiency, another slot/pole combination is considered. A three-phase 8/6 pole DSPMM with larger equivalent permeance and shorter magnetic path than 6/4 pole one is proposed [9]. A special magnetic bridge in shunt each PM pole maintains the stator lamination in its entireness, but also amplifies PM flux effect [10]. Thus, the torque per PM volume can be greatly enhanced. Furthermore, for a novel defined DSPMM, an extra winding is located in the rotor slots as armature winding which can fully utilize rotor slot area, resulting in torque enhancement. The torque ripple is greatly suppressed by selecting proper slot/pole combination [11].

A plenty of studies have been investigated to improve the torque density and reduce the torque ripple of DSPMMs. In [12], a biased flux PM machine (BFPMM) which has the similar structure as DSPMM is a promising solution. The difference lies in for BFPMM, the number of stator teeth between adjacent PMs is one, while for DSPMM, the number of stator teeth between adjacent PMs is more than one. For BFPMM, each coil has symmetrical flux path, resulting in three phase symmetry. Meanwhile, special slot-pole combination is selected in DSPMM to decrease the harmonics of flux linkage and back-EMF to some extent, leading to smaller torque ripple. However, the torque density is relatively small comparing with BFPMM. In [13-15], a novel DSPMM with special slot/pole combination and winding connection is proposed to improve the torque density as well as minimize the torque ripple. All coils wounded on each four small teeth under each main tooth are evenly allocated to three phases, three phase are symmetrical even through the different flux path of the four small teeth under each main tooth. However, there is no comprehensive study of magnetic flux and inductance analysis of this kind of machines.

Slot-PM machines, having PMs in the slot opening have been investigated in recent years. Radial magnetized slot PMs are applied to add extra PM torque with flux modulation effect [16-

Manuscript received Dec 31, 2021; revised May 10, 2022; accepted June 18, 2022. This work was supported by NSFC of China under Project 52077187 and in part by the Research Grant Council, Hong Kong, China, under Project Polyu 152109/20E and 152143/18E. (*Corresponding author: Shuangxia Niu)*

Jifu Jiang, Shuangxia Niu are with the Department of Electrical Engineering, The Hong Kong Polytechnic University, Hong Kong, China (email: 20032118r@connect.polyu.hk; eesxniu@polyu.edu.hk). Xing Zhao is with the Department of Electronic Engineering, The University of York, York, UK (email: xing.zhao@york.ac.uk).

Color versions of one or more of the figures in this paper are available online at http://ieeexplore.ieee.org.

17]. Tangential magnetized slot PMs are used to relieve stator saturation, thus boosting torque density as well as improving stator core utilization factor [18-24]. Recently, a novel hybrid reluctance machine is proposed to make use of both radial and tangential slot PMs [25]. However, few study of slot PMs are focused on the biased magnetic flux machine.

In this paper, slot PMs are newly employed in the biased flux DSPM machine to build a novel parallel-excited dual-PM reluctance machine (DPM-RM) with enhanced torque and efficiency performance. In Section II, the machine structure and operation principle are introduced. Also, the flux analysis and inductance analysis are illustrated in detail. In Section III, the leading design parameters are optimized and determined to obtain maximum torque and minimum torque ripple. Yoke PMs and slot PMs distributions are optimized with the given total amount of PMs. An optimal machine without PM volume limit is further used for quantitative analysis. In Section IV, the finite-element analysis (FEA) is used to compare the electromagnetic performance of DPM-RM without slot PMs and with slot PMs. Also, the proposed DPM-RM is compared with the existing variable reluctance machine (VRM) [26]. Finally, experiments are carried out in Section V and conclusions are drawn in Section VI.

II. Machine Structure and Operation Principle

A. Machine Structure

Fig. 1 shows the structure of the proposed parallel-excited DPM-RM, which comprises a 24-slot stator and a 28-pole rotor. The rotor is composed of only iron core with salient poles, which can provide mechanical robustness and reliability. The stator consists of all excitation sources, including AC armature winding, tangential magnetized slot PMs and yoke PMs. The AC armature winding adopts a doubly-layer concentrated winding connections as showed in Fig. 2.

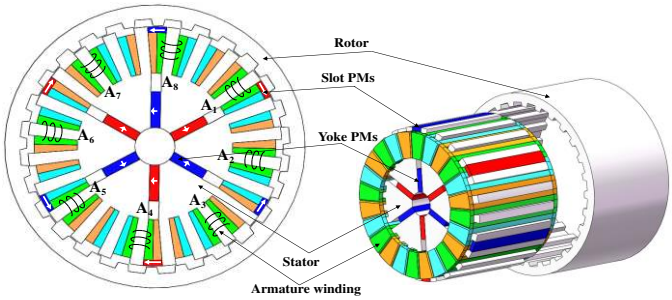

Fig. 1. Structure of the proposed machine.

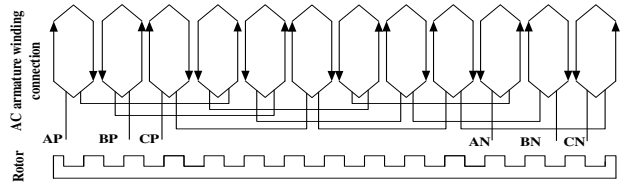

Fig. 2. Winding connection (P and N refers to polar distribution).

The main merits of proposed machine are listed as following.

1) The PMs in the stator yoke and slot openings are located in parallel and magnetized in the same tangential direction. Since slot PMs and yoke PMs have the same pole pair number and share the same parallel magnetic circuit, the magnetic flux excited by two PMs can be superimposed in the airgap, thus effectively strengthening the flux variation, and improving the back-EMF and torque accordingly.
2) In this proposed design, with special slot/pole combination, DC component and even order harmonics in the phase flux are eliminated, which makes phase flux linkage more sinusoidal. In the meantime, variation of self-inductance is greatly reduced with odd order harmonics of phase self-inductance removed, resulting in small torque ripple.
3) The slot-PM flux passing through the stator yoke can partially relieve the stator core saturation, thus improving stator core utilization factor and enhancing torque density.

B. Slot-pole Combination

Due to the conventional combination of stator pole number, rotor pole number, yoke/slot PM pole number, as well as phase number are not carefully designed, traditional biased flux stator-PM machine suffers from not only asymmetric flux linkage and back-EMF, but also large self-inductance variation and torque ripple. Two criteria are presented to solve abovementioned problems.

Firstly, every phase comprises coils which should be distributed in all locations relative to each yoke/slot PM pole [10]. Hence, the number of coils under a yoke/slot PM pole should be different from the number of phases, which can be expressed as:

$$(m+k)N_{pm} = N_s \tag{1}$$

where m is the phase number, k is a positive integer and $k < m$. Meanwhile, N_{pm} and N_s present yoke/slot PM pole number and stator pole number.

Secondly, in order to avoid single-sided magnetic force, the difference between the number of rotor pole and stator pole is a multiple of two. The second criterion can be denoted as:

$$N_r = N_s \pm 2k_1 \tag{2}$$

where, k_1 is a positive integer. If $m = 3$ and $N_{pm} = 6$ is given, let $k = 1$, then $N_s = 24$ is deduced from (1). In order to make $N_r > N_s$, for the proposed machine, let $k_1 = 2$, then $N_r = 28$ is adopted from (2). In this case, slot/pole combination is 24/28.

C. Flux analysis

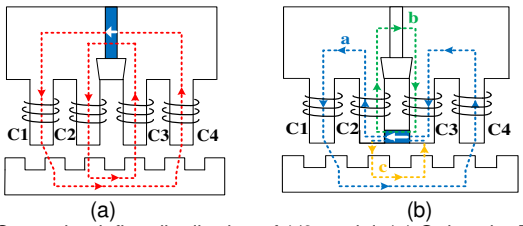

Fig. 3. Open-circuit flux distribution of 1/6 model. (a) Only yoke PMs. (b) Only slot PMs (Blue line a: main flux linkage produces torque; green line b: flux leakage relieves core saturation; yellow line c: flux leakage).

Fig. 3 presents an open-circuit flux distribution of 1/6 machine model under different excitation sources. As shown in Fig. 3, coils C1, C2, C3 and C4 are placed under four different positions relative to each yoke/slot PM pole. The positive flux direction can be defined as flux flowing from rotor to stator while the negative flux direction can be defined as flux flowing

from stator to rotor. When only yoke PMs is used as denoted in Fig. 3(a), the flux linkage passes through the airgap, and links with the stator winding and the rotor. It can be seen that the flux directions in C1 and C2 are negative, while the flux directions in C3 and C4 are positive. When only slot PMs is applied as shown in Fig. 3(b), the flux linkage has the main path and leakage flux paths. For the main path, as shown in blue line a, the main linkage passes through the adjacent teeth, distant teeth, airgap, and links with the stator winding and the rotor, which can produce effective torque. For the flux leakage paths, there are two magnetic circuit loops. Some flux leakage goes into the airgap and rotor directly, as shown in yellow line c, and other passes through the yoke PMs and only links with the stator, which cannot provide efficient torque but can relieve stator core saturation, especially at the teeth bottom, as shown in green line b. It can be noticed that flux directions in C1 and C3 are negative, while flux direction in C2 and C4 are positive.

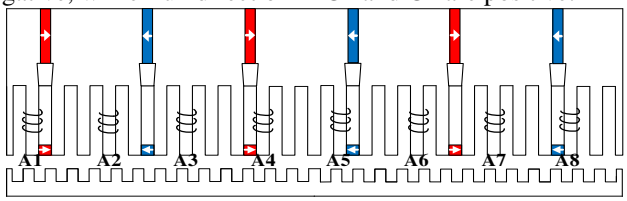

Fig. 4. Phase A coil distribution.

As shown in the linear machine model of Fig. 4, phase A is formed with eight coils, from coils A1 to A8. Among them, A1 to A4 are connected in series, which are categorized as group 1. A5 to A8 are connected in series, which are categorized as group 2. Group 1 and group 2 are reversely connected. In this case, A1 and A5, A2 and A6, A3 and A7, A4 and A8 have the same flux linkage waveforms. Hence, phase A flux linkage is twice the total flux linkage of coils A1, A2, A3, and A4. It is worth noting that, coils A1, A2, A3, and A4 are placed at four different positions relative to each yoke/slot PM pole. Comparing Fig. 3 with Fig. 4, coil A1 is corresponding to C3 since they have the same position relative to each yoke/slot PM pole. Similarly, coil A2 is corresponding to C1, coil A3 is corresponding to C4, and coil A4 is corresponding to C2. The only flux linkage discrepancy between the corresponding coils lies in the phase difference. According to coils A1, A2, A3 and A4 distribution, the flux linkage phase difference between them is equal to zero, which will be illustrated in the following.

The open-circuit flux path analysis is essential to explain the working principle of the proposed machine. Fig. 5 shows qualitative flux waveform in coils A1 to A4. Ψ_{yA1}, Ψ_{yA2}, Ψ_{yA3} and Ψ_{yA4} represent the flux linkage excited by yoke PMs in coil A1, A2, A3, and A4 respectively. Ψ_{sA1}, Ψ_{sA2}, Ψ_{sA3} and Ψ_{sA4} denote the flux linkage excited by slot PMs in coil A1, A2, A3, and A4 respectively. Ψ_{A1}, Ψ_{A2}, Ψ_{A3} and Ψ_{A4} denote the flux linkage excited by both excitations in coil A1, A2, A3, and A4 respectively. In Fig. 5(a), adjacent yoke PM and slot PM have the same magnetizing direction, and coil A1 shares the same mechanical angle with them. Therefore, Ψ_{yA1} and Ψ_{sA1} are entirely in phase with each other, thus Ψ_{A1} can obtain the maximum flux variation with the parallel excitation of both PMs. In addition, A1 is corresponding to C3, thus Ψ_{yA1} is positive while Ψ_{sA1} is negative. Hence, for coil A1, flux linkage of slot PMs can reduce the positive biased flux linkage from the yoke PMs in the stator teeth.

Similarly, as presented in Fig. 5(b), for coil A2, Ψ_{A2} can attain the maximum flux variation, and flux linkage of slot PMs Ψ_{sA2} can greatly boost the negative biased flux linkage of yoke PMs Ψ_{yA2}. As shown in Fig. 5(c), for coil A3, Ψ_{A3} can achieve the maximum flux variation, and flux linkage of slot PMs Ψ_{sA3} can greatly boost the positive biased flux linkage of yoke PMs Ψ_{yA3}. As exhibited in Fig. 5(d), for coil A4, Ψ_{A4} can reach the maximum flux variation, and flux linkage of slot PMs Ψ_{sA4} can reduce the negative biased flux linkage of yoke PMs Ψ_{yA4}.

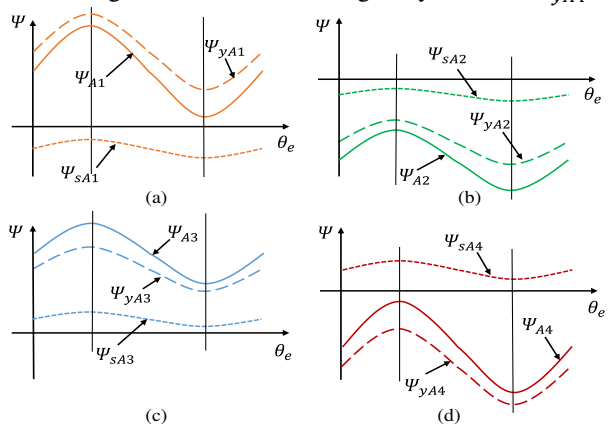

Fig. 5. Open-circuit flux linkage. (a) A1. (b) A2. (c) A3. (d) A4.

In summary, slot-PM flux boosts yoke-PM flux in coils A2 and A3 which can be seen in Fig. 5(b) and Fig. 5(c), while slot-PM flux reduces yoke-PM flux in coils A1 and A4 as shown in Fig. 5(a) and Fig. 5(d). However, the flux of yoke PMs and slot PMs attain the maximum value and minimum value at the same time, thus flux variation of them are superimposed to attain a larger value.

As shown in Fig. 6, the flux linkages excited by both PMs in coil A1, A2, A3 and A4 are entirely in phase with each other, phase A flux linkage (Ψ_A) is twice the total flux linkage of coils A1, A2, A3, A4 (Ψ_{A1}, Ψ_{A2}, Ψ_{A3}, Ψ_{A4}). Additionally, since coils A1 and A4, A2 and A3 are located in symmetrical positions with respect to adjacent yoke PM pole and slot PM pole, flux-linkage DC bias in coils A1 and A4 have the same amplitude, but differ in flux direction, thus can counteract each other as shown in Fig. 5(a) and Fig. 5(d). Similarly, the flux-linkage DC bias in coils A2 and A3 can also compensate each other as shown in Fig. 5(b) and Fig. 5(c). Therefore, biased DC components are eliminated in the phase A flux linkage as shown in Fig. 6, and torque ripple can be greatly reduced.

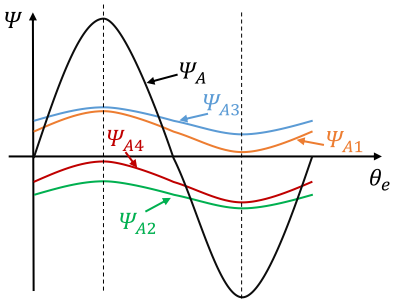

Fig. 6. Open-circuit flux linkage.

For yoke PMs, the flux linkage in four different coils A1, A2, A3 and A4 are denoted as Ψ_{yA1}, Ψ_{yA2}, Ψ_{yA3} and Ψ_{yA4}, which can be expressed as

$$\begin{cases} \psi_{\mathrm{yA1}} = \psi_{yDCA1} + \sum_{n=1}^{+\infty} \psi_{yACA1n} \cos(nP_r\theta_r) \\ \psi_{\mathrm{yA2}} = -\left\{ \psi_{yDCA2} + \sum_{n=1}^{+\infty} \psi_{yACA2n} \cos[nP_r(\theta_r - \frac{2\pi}{P_s} \times 3)] \right\} \\ \psi_{\mathrm{yA3}} = \psi_{yDCA3} + \sum_{n=1}^{+\infty} \psi_{yACA3n} \cos[nP_r(\theta_r - \frac{2\pi}{P_s} \times 6)] \\ \psi_{\mathrm{yA4}} = -\left\{ \psi_{yDCA4} + \sum_{n=1}^{+\infty} \psi_{yACA4n} \cos[nP_r(\theta_r - \frac{2\pi}{P_s} \times 9)] \right\} \end{cases} \tag{3}$$

where Ψ_{yDCA1} , Ψ_{yDCA2} , Ψ_{yDCA3} and Ψ_{yDCA4} are the DC components of flux linkage excited by yoke PMs in coils A1, A2, A3 and A4. Ψ_{yACA1n}, Ψ_{yACA2n}, Ψ_{yACA3n} and Ψ_{yACA4n} are the magnitude of *n*th harmonics of flux linkage excited by yoke PMs in coils A1, A2, A3 and A4. P_r represents salient pole number of rotor while P_s denotes stator slot number. n represents *n*th harmonics.

For slot PMs, the flux linkage in four different coils A1, A2, A3 and A4 are denoted as Ψ_{sA1}, Ψ_{sA2}, Ψ_{sA3} and Ψ_{sA4}, which can be presented as

$$\begin{cases} \psi_{\mathrm{sA1}} = -\psi_{sDCA1} + \sum_{n=1}^{+\infty} \psi_{sACA1n} \cos(nP_r\theta_r) \\ \psi_{\mathrm{sA2}} = -\left\{ \psi_{sDCA2} + \sum_{n=1}^{+\infty} \psi_{sACA2n} \cos[nP_r(\theta_r - \frac{2\pi}{P_s} \times 3)] \right\} \\ \psi_{\mathrm{sA3}} = \psi_{sDCA3} + \sum_{n=1}^{+\infty} \psi_{sACA3n} \cos[nP_r(\theta_r - \frac{2\pi}{P_s} \times 6)] \\ \psi_{\mathrm{sA4}} = \psi_{sDCA4} - \sum_{n=1}^{+\infty} \psi_{sACA4n} \cos[nP_r(\theta_r - \frac{2\pi}{P_s} \times 9)] \end{cases} \tag{4}$$

where Ψ_{sDCA1} , Ψ_{sDCA2} , Ψ_{sDCA3} and Ψ_{sDCA4} are the DC components of flux linkage excited by slot PMs in coils A1, A2, A3 and A4. Ψ_{sACA1n}, Ψ_{sACA2n}, Ψ_{sACA3n} and Ψ_{sACA4n} are the magnitude of *n*th harmonics of flux linkage excited by slot PMs in coils A1, A2, A3 and A4.

Due to coils A1 and A4, A2 and A3 are located in symmetrical positions with respect to a yoke PM pole and a slot PM pole, $\Psi_{yDCA1} = \Psi_{yDCA4}$, $\Psi_{yDCA2} = \Psi_{yDCA3}$, $\Psi_{yACA1n} = \Psi_{yACA4n}$, $\Psi_{yACA2n} = \Psi_{yACA3n}$, $\Psi_{sDCA1} = \Psi_{sDCA4}$, $\Psi_{sDCA2} = \Psi_{sDCA3}$, $\Psi_{sACA1n} = \Psi_{sACA4n}$, $\Psi_{sACA2n} = \Psi_{sACA3n}$.

For dual PMs, the flux linkage in coils A1, A2, A3, and A4 can be denoted as

$$\begin{cases} \psi_{\mathrm{A1}} = \psi_{\mathrm{yA1}} + \psi_{\mathrm{sA1}} \\ \quad = (\psi_{yDCA1} - \psi_{sDCA1}) + \sum_{n=1}^{+\infty} (\psi_{yACA1n} + \psi_{sACA1n}) \cos(nP_r\theta_r) \\ \psi_{\mathrm{A2}} = \psi_{\mathrm{yA2}} + \psi_{\mathrm{sA2}} \\ \quad = -(\psi_{yDCA2} + \psi_{sDCA2}) \\ \quad\quad - \sum_{n=1}^{+\infty} (\psi_{yACA2n} + \psi_{sACA2n}) \cos[nP_r(\theta_r - \frac{2\pi}{P_s} \times 3)] \\ \psi_{\mathrm{A3}} = \psi_{\mathrm{yA3}} + \psi_{\mathrm{sA3}} \\ \quad = (\psi_{yDCA3} + \psi_{sDCA3}) \\ \quad\quad + \sum_{n=1}^{+\infty} (\psi_{yACA3n} + \psi_{sACA3n}) \cos[nP_r(\theta_r - \frac{2\pi}{P_s} \times 6)] \\ \psi_{\mathrm{A4}} = \psi_{\mathrm{yA4}} + \psi_{\mathrm{sA4}} \\ \quad = -(\psi_{yDCA4} - \psi_{sDCA4}) \\ \quad\quad - \sum_{n=1}^{+\infty} (\psi_{yACA4n} + \psi_{sACA4n}) \cos[nP_r(\theta_r - \frac{2\pi}{P_s} \times 9)] \end{cases} \tag{5}$$

According to (5), the flux linkage excited by yoke PMs and slot PMs is superposed for coils A2 and A3 while which is counteracted for coils A1 and A4. Additionally, through adding Ψ_{A1} to Ψ_{A4} , phase A flux linkage can be expressed as

$$\begin{aligned} \psi_A &= 2\times(\psi_{\mathrm{A1}} + \psi_{\mathrm{A2}} + \psi_{\mathrm{A3}} + \psi_{\mathrm{A4}}) \\ &= -4\times \sum_{n=1,3,5\ldots}^{+\infty} (\psi_{yACA1n} + \psi_{sACA1n}) \sin(9n\pi \frac{P_r}{P_s}) \sin[nP_r(\theta_r - \frac{9\pi}{P_s})] \\ &\quad + 4\times \sum_{n=1,3,5\ldots}^{+\infty} (\psi_{yACA2n} + \psi_{sACA2n}) \sin(3n\pi \frac{P_r}{P_s}) \sin[nP_r(\theta_r - \frac{9\pi}{P_s})] \end{aligned} \tag{6}$$

According to (6), the DC components and the even order harmonics of phase A flux linkage are eliminated completely. It is worth noticing that flux variation is effectively strengthened with parallel-excited yoke PMs and slot PMs.

The higher order harmonics which are much smaller comparing with fundamental wave, can be ignored. Thus, the phase flux linkage is nearly sinusoidal with the special slot/pole combination and winding connection.

D. Inductance analysis

Machine inductances are analyzed to verify that the salient effect is greatly reduced in the proposed machine. Take the inductance of phase A for example. The self-inductances of coils A1 to A4 can be written as

$$\begin{cases} L_{\mathrm{A1}} = L_{DCA1} + \sum_{n=1}^{+\infty} L_{ACA1n} \cos(nP_r\theta_r) \\ L_{\mathrm{A2}} = L_{DCA2} + \sum_{n=1}^{+\infty} L_{ACA2n} \cos[nP_r(\theta_r - \frac{2\pi}{P_s} \times 3)] \\ L_{\mathrm{A3}} = L_{DCA3} + \sum_{n=1}^{+\infty} L_{ACC3n} \cos[nP_r(\theta_r - \frac{2\pi}{P_s} \times 6)] \\ L_{\mathrm{A4}} = L_{DCA4} + \sum_{n=1}^{+\infty} L_{ACA4n} \cos[nP_r(\theta_r - \frac{2\pi}{P_s} \times 9)] \end{cases} \tag{7}$$

where L_{DCA1} , L_{DCA2} , L_{DCA3} and L_{DCA4} are the DC components of self-inductances of coils A1, A2, A3 and A4. L_{ACA1n}, L_{ACA2n}, $L_{ACA3n}$and L_{ACA4n} are the magnitude of *n*th harmonics of self-inductances of coils A1, A2, A3 and A4.

Coils A1 and A4, A2 and A3 are located in symmetrical positions with respect to adjacent yoke PM pole and slot PM pole, therefore $L_{DCA1} = L_{DCA4}$, $L_{DCA2} = L_{DCA3}$, $L_{ACA1n} = L_{ACA4n}$, $L_{ACA2n} = L_{ACA3n}$. In addition, the mutual inductances among A1, A2, A3 and A4, which are quite small comparing with self-inductances, can be ignored. The self-inductance of phase A L_A is the twice the sum of coils A1, A2, A3 and A4 self-inductances L_{A1}, L_{A2}, L_{A3} and L_{A4}, which can be denoted as

$$\begin{aligned} L_A &= 2\times(L_{\mathrm{A1}} + L_{\mathrm{A2}} + L_{\mathrm{A3}} + L_{\mathrm{A4}}) \\ &= 4\times(L_{DCA1} + L_{DCA2}) \\ &\quad + 4\times \sum_{n=2,4,6\ldots}^{+\infty} L_{ACC1n} \cos(9n\pi \frac{P_r}{P_s}) \cos[nP_r(\theta_r - \frac{9\pi}{P_s})] \\ &\quad + 4\times \sum_{n=2,4,6\ldots}^{+\infty} L_{ACC2n} \cos(3n\pi \frac{P_r}{P_s}) \cos[nP_r(\theta_r - \frac{9\pi}{P_s})] \end{aligned} \tag{8}$$

According to (8), with special slot/pole combination, the odd order harmonics of phase A self-inductance are eliminated thoroughly, while the DC component and even order harmonics of phase A self-inductance remain. Since the magnitudes of high order harmonics are very small, the phase A self-inductance is nearly a constant value with DC component. In other word, with special slot/pole combination, the salient

effect of the proposed machine is greatly reduced with a constant phase self-inductance.

III. Design Optimization

A. Combined GA and FEA Optimization

In order to optimize the machine performance, the leading dimension parameters need to be further optimized.

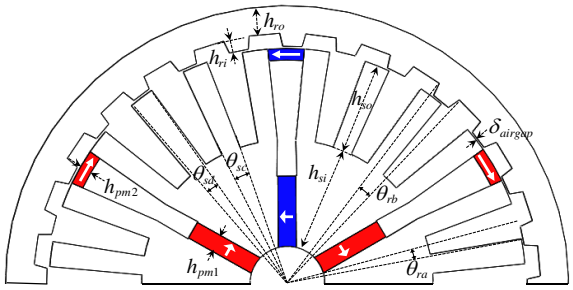

Fig. 7. Dimension parameters of the proposed machine.

TABLE I
INITIAL DIMENSION PARAMETERS OF THE PROPOSED MACHINE

Symbol	Parameter	Unit	Value
R_{ro}	Outer radius of rotor	mm	75
R_{si}	Inner radius of stator	mm	10
h_{ro}	Height of rotor yoke	mm	Variable
h_{ri}	Height of rotor slot	mm	Variable
h_{so}	Height of stator slot	mm	Variable
h_{si}	Height of stator yoke	mm	Variable
l	Stack length	mm	80
δ_{airgap}	Airgap length	mm	0.6
h_{pm1}	Height of yoke-PMs	mm	Variable
h_{pm2}	Height of slot-PMs	mm	Variable
θ_{ra}	Arc of rotor tooth top	rad	Variable
θ_{rb}	Arc of rotor tooth bottom	rad	Variable
θ_{sc}	Arc of stator tooth bottom	rad	Variable
θ_{sd}	Arc of stator tooth top	rad	Variable

Due to the large number of dimension parameters, it is time-consuming to optimize all the parameters through traditional analysis method. Hence, this paper applies genetic algorithm (GA). GA is derived from biology concept, which can find the optimal result by imitating the effect of nature selection. Referring to nature selection process, GA has three operation factors, namely, reproduction, crossover, and mutation. Reproduction generates the most adaptive individual survival, while crossover and mutation expand the searching scope. GA, which is an excellent method for optimization, communicates with FEA to realize combined optimization.

The main purpose of this optimization is to attain relatively higher average torque and lower torque ripple. The constraint is outer diameter of machine. The initialization of GA is performed as, a population of 50 elements, maximum generation number of 20, crossover factor of 0.8 and mutation factor of 0.2. Some dimensional parameters are labeled in Fig. 7, with initial dimension parameter values presented in Table I.

A multi-objective optimization can cause plenty of unsuitable cases. For example, some elements have relatively high average torque and high torque ripple, while some have relatively low torque ripple and low average torque. A few of relative optimal elements are found at the turning points, which possess relatively high average torque and low torque ripple.

B. Slot PMs and Yoke PMs Distribution under the Given Total Amount of PMs

If the total amount of PMs is constant, it is important to determine the distribution of PMs in stator yoke and slot openings. With this objective, several optimizations are carried out with given total amount of PMs. The axial length of machine is fixed at 80 mm.

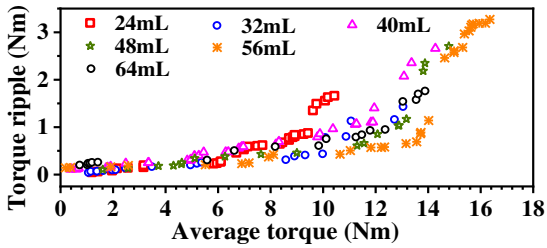

Fig. 8. Optimized results of the last generation with different PM volume.

TABLE II
OPTIMAL PM DISTRIBUTION WITH DIFFERENT TOTAL PMS VOLUME

Total PM volume (mL)	Yoke-PM volume (mL)	Slot-PM volume (mL)	Slot-PM ratio	Torque (Nm)	Torque Ripple (Nm)	Torque/ volume (Nm/mL)
24	14.261	9.768	0.4070	9.11	0.83	0.38
32	21.326	10.694	0.3342	10.08	0.78	0.32
40	31.728	8.400	0.2100	10.37	0.96	0.26
48	45.970	2.198	0.0458	12.07	0.85	0.25
56	49.992	6.163	0.1100	13.16	0.65	0.24
64	48.000	16.000	0.2500	12.36	0.95	0.19

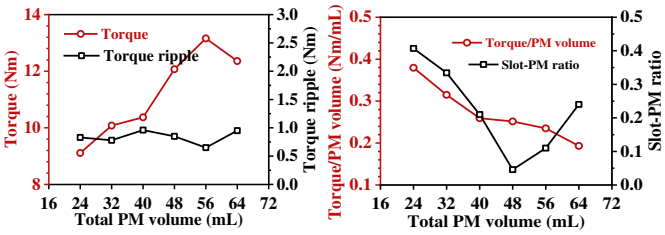

Fig. 9. Torque, torque ripple, slot-PM ratio, and torque per PM volume.

Fig. 8 shows the optimization results with different total PM volume. Table II gives optimal values according to given total PM volume. Fig. 9 denotes torque, torque ripple, torque per volume and slot-PM ratio with different total PM volume. In this paper, slot-PM ratio is defined as the slot-PM volume against total PM volume. As shown in Fig. 9(a), average torque advances when total amount of PMs increases from 24mL to 56mL, while average torque reduces when total amount of PMs increases from 56mL to 64mL. In addition, torque ripple has no relationship with total PM volume. As presented in Fig. 9(b), torque per PM volume decreases with the increase of the total PM volume. In addition, slot-PM ratio decreases when total amount of PMs increases from 24mL to 48mL, while slot-PM ratio enhances when total amount of PMs increases from 48mL to 64mL. In addition, Therefore, with given total amount of PMs, we can determine slot PMs and yoke PMs amount according to Table II and Fig. 9. Also, to attain maximum torque, we can choose 56mL total PM volume. Torque per PM volume achieves relatively high value when the total PM volume is relatively low.

C. Design optimization with no PM volume limitation

If the total PM volume is not limited, the optimization results of last generation is obtain as shown in Fig. 10. The point denoted by the red circle is the selected optimal case and corresponding dimension parameter values are presented in Table III. In this case, the total PM volume is 58.272 mL with 13.77 Nm steady torque and 0.2 slot-PM ratio, which agrees well with above analysis.

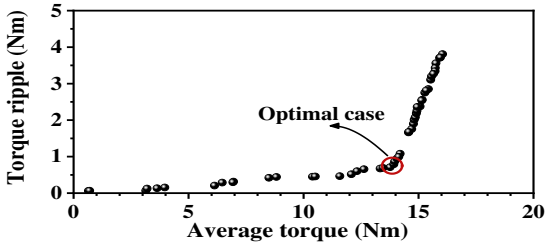

Fig. 10. Optimization results of last generation.

TABLE III
DIMENSION PARAMETERS, BOUNDARY LIMITS AND OPTIMAL VALUES

	Parameter	Lower Limit (mm)	Lower Limit (mm)	Optimization (mm)
Out rotor	h_{ro}	4	16	7.45
	h_{ri}	2	12	3.50
	θ_{ra}	0.08	0.16	0.0800
	θ_{rb}	0.10	0.18	0.1024
Inner stator	h_{so}	9	25	24.65
	h_{si}	10	40	28.80
	θ_{sc}	0.10	0.20	0.1336
	θ_{sd}	0.08	0.18	0.1074
Yoke-PMs	h_{pm1}	0.0001	10	4.81
Slot-PMs	h_{pm2}	0.0001	9	3.14

IV. ELECTROMAGNETIC PERFORMANCE ANALYSIS

A. Flux Distribution and Harmonic Analysis with FEA

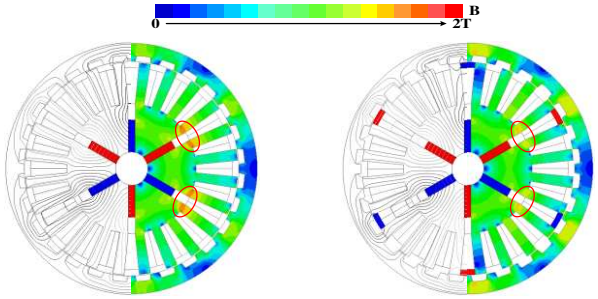

Fig. 11. Open-circuit flux distribution under different excitation status. (a) Only yoke PMs. (b) Both yoke PMs and slot PMs.

Fig. 11 shows the open-circuit flux distribution under different excitation status. It is shown that both yoke PMs and slot PMs have the same pole pair number and share the same magnetic circuit. As for yoke PMs, the flux passes through the stator, airgap, links the rotor, and then goes back to stator, which is denoted in Fig. 11(a). The flux produced by dual PMs has no phase shifts and can be superimposed to attain maximum variation as shown in Fig. 11(b), which results in larger back-EMF and steady torque. Noticeably, as shown in red circles in Fig. 11(a) and Fig. 11(b), stator teeth bottom near the PM pole becomes less saturated with the employment of the slot PMs.

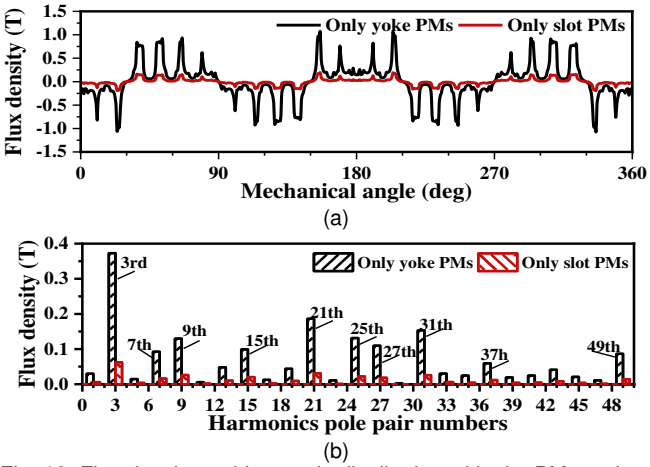

Fig. 12. Flux density and harmonic distribution with slot PMs and yoke PMs. (a) Airgap flux density waveforms. (b) Harmonic distribution.

The airgap flux density and harmonic distribution under different excitation sources are plotted in Fig. 12. Comparing Fig. 12(a) with Fig. 12(b), the airgap flux density waveforms under only yoke PMs and only slot PMs excitation have the same trend but only differ in amplitude. It is the same as harmonic distribution. This verifies previous conclusion that slot-PM main flux and yoke-PM flux have the same pole pair number and share a parallel magnetic circuit. In this way, the flux variation strengthening can be realized with dual PMs.

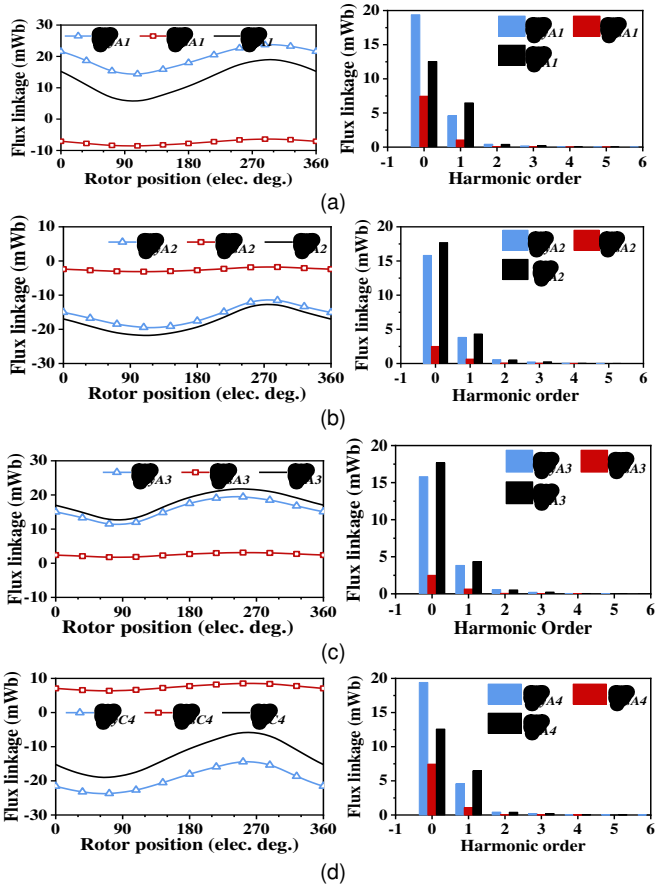

Fig. 13. Open-circuit flux linkage waveforms and harmonics. (a) Coil A1. (b) Coil A2. (c) Coil A3. (4) Coil A4.

The open-circuit flux linkage waveforms and corresponding harmonics in coils A1, A2, A2 and A4 are presented in Fig. 13. For coil A1, slot-PM flux linkage can reduce the positive biased yoke-PM flux linkage. For coil A2, slot-PM flux linkage can largely boost the negative yoke-PM flux linkage. For coil A3, slot-PM flux linkage can enhance the positive yoke-PM flux linkage. For coil A4, slot-PM flux linkage can decrease the negative yoke-PM flux linkage. Since coils A2 and A3 are far from the PM poles, while A1 and A4 are close to PM poles, slot-PM flux reduces the yoke-PM flux in the coils near the PM poles and enhances the yoke-PM flux in the coils far from PM poles. However, for coils A1 to A4, flux variation of yoke PMs can be enhanced with the employment of slot PMs.

The open-circuit flux linkage waveforms and corresponding harmonics of phase A and its coils are denoted in Fig. 14. It can be found that flux linkages of coils A1, A2, A3 and A4 are totally in phase with each other. Due to coil flux linkages have no phase shift with each other, phase A flux linkage can obtain the maximum flux linkage variation. Moreover, DC components of flux linkage in coils A1 and A4 have the same amplitude but differ in direction. The same as DC components of flux linkage in coils A2 and A3. Furthermore, DC component and even order harmonics of flux linkage in phase A are eliminated which is in accordance with aforementioned flux analysis. Noticeably, the phase A flux linkage is perfect sinusoidal waveform with the special slot/pole combination.

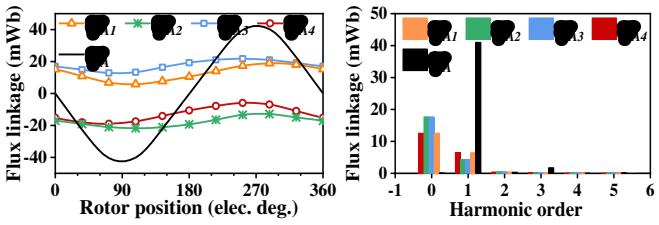

Fig. 14. Open-circuit flux linkage. (a) Waveforms. (b) Harmonics.

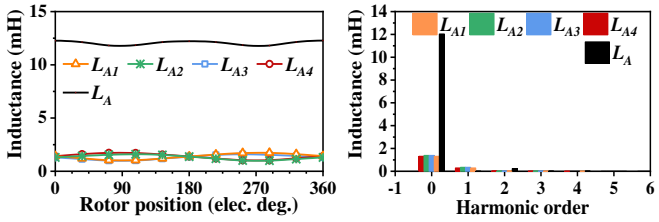

Fig. 15. Self-inductance. (a) Waveforms. (b) Harmonics.

The open-circuit self-inductance waveforms and harmonics of phase A and its coils are shown in Fig. 15. It can be noticed that the phase A self-inductance has only minor variation as shown in Fig. 15(a), which showcases a non-salient effect with small torque ripple. In addition, the phase A self-inductance has only DC component and even order harmonics, which is consistent with aforementioned inductance analysis.

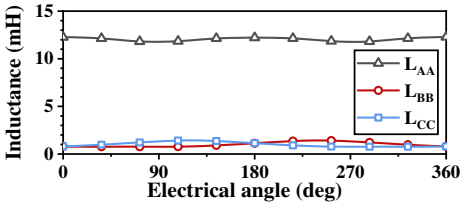

Fig. 16. Open-circuit self- and mutual inductance of phase A.

The open-circuit self and mutual inductance of phase A are presented in Fig. 16. The mutual inductances are pretty small comparing with self-inductance and can be neglected, which is consistent with abovementioned analysis.

B. Thermal and Demagnetization Analysis

Since slot PMs are near the stator poles and armature winding while yoke PMs are buried in the yoke of the inner stator, the heat extraction is needed to be seriously considered. Assuming the ambient temperature is 25 ℃, through assigning the losses of each part of the proposed machine to a 3-D modified model, temperature distribution can be shown in Fig. 17. The highest temperature in rotor core, stator core, stator PMs and armature winding are 83.6 ℃, 89.8 ℃, 89.5 ℃ and 90.2 ℃ respectively.

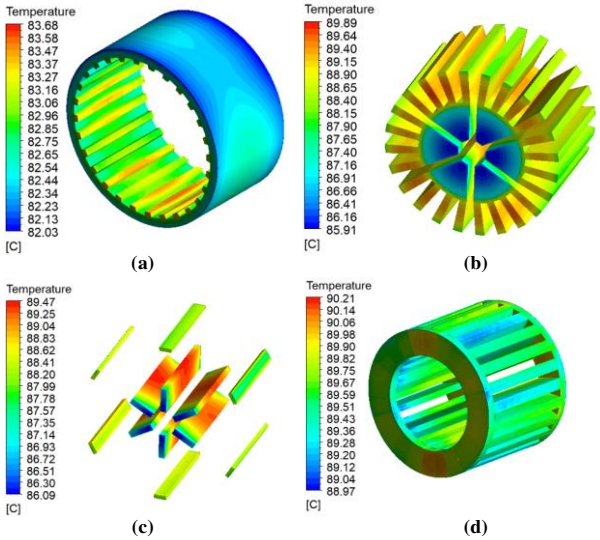

Fig. 17. Temperature distribution in each part of the proposed machine. (a) Rotor core. (b) Stator core. (c) Stator PMs. (d) Armature winding.

In order to testify the PM demagnetization withstanding capability of the proposed machine, the flux density distribution and corresponding selected point flux density variations under rated load at 90 ℃ are denoted in Fig.18. It presents that the flux density of all selected points during an electrical period exceed the irreversible demagnetization threshold value. Therefore, PM demagnetization withstand capability is pretty good under rated load condition.

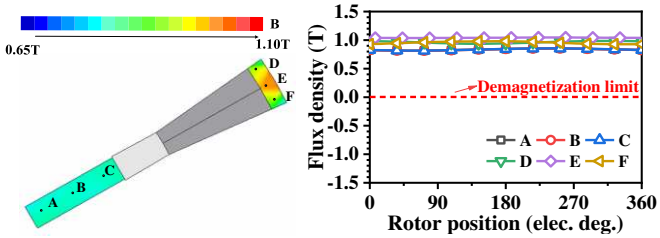

Fig. 18. PM demagnetization withstand capability under rated load at 90 ℃. (a) Flux density distributions. (Selected points). (b) Selected point flux density variations.

C. Comparative study

In order to verify better performance of the proposed DPM-RM than the existing variable reluctance machine (VRM) [26], and testify the effectiveness of slot PMs, three machines with the same outer rotor diameter, stack length, rated current density are taken into comparison as shown in Fig. 19.

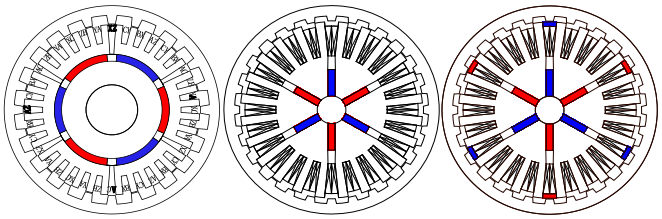

(a) (b) (c)

Fig. 19. Machines for comparison. (a) The existing VRM. (2) DPM-RM without slot PMs. (b) DPM-RM with slot PM (The proposed machine).

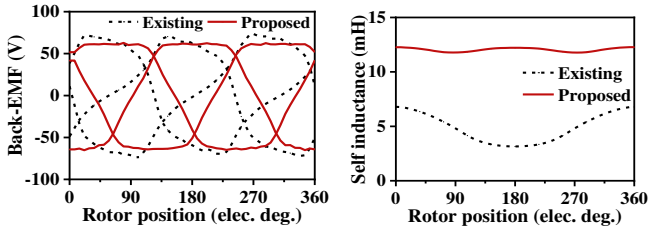

(a) (b)

Fig. 20. Open-circuit electromagnetic performance. (a) Back-EMF. (b) Self-inductance.

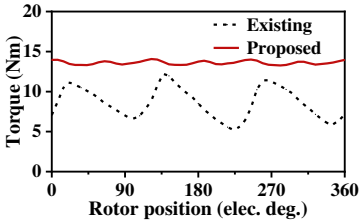

Fig. 21. On-load torque waveform.

Fig. 20 (a) gives the open-circuit back-EMF. It is obvious that the proposed machine can offer more symmetrical and trapezoidal back-EMF waveform than the existing machine. Fig. 20(b) shows the phase self-inductance waveforms. It shows that the proposed machine can provide smaller variation of self-inductance with non-salient effect, resulting in small torque ripple. Fig. 21 gives the on-load torque of two machines. The average torque of the existing and proposed machines are 8.59 Nm and 13.77 Nm respectively. The torque ripple ratios of the existing and proposed machines are 81.4% and 5.9% respectively. It verifies the proposed machine has symmetrical electromagnetic performance, smaller self-inductance variation, smaller torque ripple with special slot/pole combination and special winding connection. Therefore, the radial magnetic force is nearly zero.

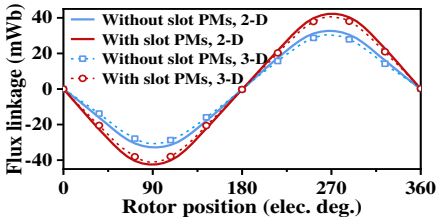

Fig. 22. Open-circuit flux linkage.

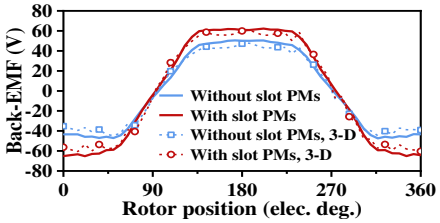

Fig. 23. Open-circuit back-EMF.

As shown in Fig. 22, the amplitudes of flux linkages of DPM-RM without slot PMs and with slot PMs are 32.7 Wb and 42.3 Wb from 2-D FEA. The open-circuit flux linkage can be increased by 29.36% with the introducing of slot PMs. The flux-linkages predicted by 3-D FEA are lower than that by 2-D FEA due to the end effects.

As denoted in Fig. 23. It has the similar conclusions as open-circuit flux linkage. The amplitudes of back-EMFs of DPM-RM without slot PMs and with slot PMs are 50.5 V and 62.3 V using 2-D FEA. The open-circuit back-EMF can be enhanced by 23.37% by adopting slot PMs. The back-EMFs predicted by 3-D FEA are lower than that by 2-D FEA due to the end effects. Fig. 24 denotes cogging torque. 3-D FEA results have larger cogging torque ripple than 2-D FEA results.

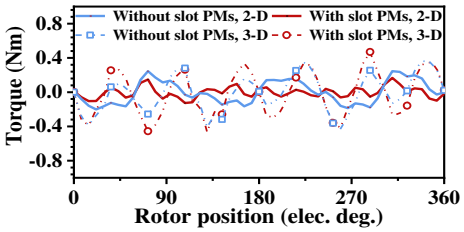

Fig. 24. Cogging torque of two machines.

The AC excitation current is given as 9 A with 6 A/mm^2 of rated current density in Fig. 25. It can be calculated that torque of DPM-RM without slot PMs and with slot PMs are 10.82 Nm and 13.77 Nm from 2-D FEA. The steady torque can be improved by 27.26% with the use of slot PMs. The steady torque using 3-D FEA is lower than that using 2-D FEA because of the end effects. The torque ripple ratio is defined as peak-to-peak value against average value. The torque ripple ratios of DPM-RM without slot PMs and with slot PMs are 10.00% and 5.05% in 2-D FEA, while are 15.07% and 11.55% in 3-D FEA. In addition, the proposed machine has higher torque and lower torque ripple ratio, which verifies that the proposed machine has excellent reliability according to the vibration generating by torque ripple.

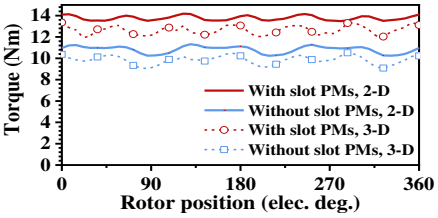

Fig. 25. Steady torque of two machines.

Considering the inverter voltage limit and current limit, the efficiency maps of DPM-RM without and with slot PMs under the peak phase current of 18 A and limited DC voltage of 180 V are presented in Fig. 26. The DPM-RM with slot PMs has the higher efficiency both in low-speed constant torque and high-speed constant power regions, which is suitable for electrical vehicle and wind power generation applications.

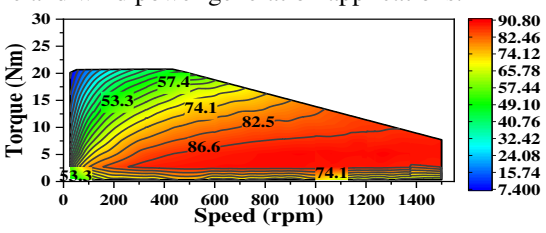

(a)

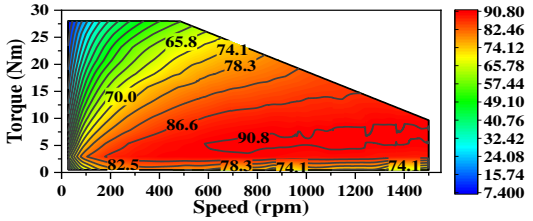

(b)

Fig. 26. Efficiency map. (a) Without slot PMs. (b) With slot PMs. (I_{max}=18 A, U_{dc}=180 V).

V. Experimental Validation

A parallel excited DPM-RM prototype with dimension parameters given in Table I and Table III is manufactured. And the electromagnetic performances of the prototype are tested. Fig. 27 shows the stator core, winding connection, and robust rotor respectively. A test platform is established as shown in Fig. 28, which includes prototype, dynamometer, oscilloscope, DC power supply, dSPACE, inverter, as well as control panel. Also, the details of parts in test platform are represented in Table IV. To obtain open-circuit back-EMF, the prototype is dragged by servo drive motor with 600 rpm rated speed, and back-EMF is measured by the oscilloscope. To obtain on-load characteristics, such as steady torque and total loss, the prototype is supplied with three-phase currents from dSPACE.

The drive system of the proposed machine comprises dc power supply, a large capacitor, a three-phase inverter for armature windings. The conventional vector control circuit adopts speed outer loop and current inner loop. Space vector pulse width modulation (SVPWM) is used to realize operation target. Since the proposed machine has non-salient effect, conventional I_d=0 control can be applied.

(a) (b) (c)

Fig. 27. Prototype. (a) Stator core. (b) Winding connection. (c) Rotor.

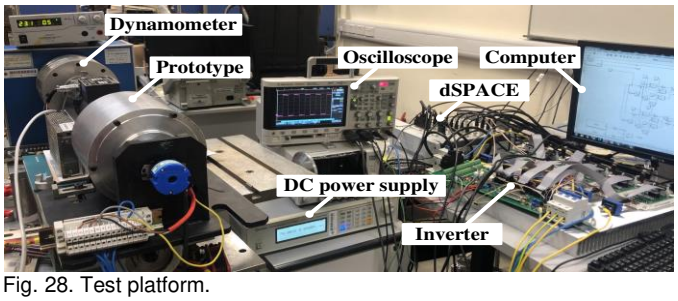

Fig. 28. Test platform.

TABLE IV
The Details of Parts in Test Platform

Device	Model	Device	Model
Prototype	Machine	dSPACE	Microlabbox
Dynamometer	CF200KS	DC power supply	62024P-600-8
Oscilloscope	DSO-X 2022A	Inverter	Self-built
Computer	Dell	Rotary encode	TS5214N8566

The measured open-circuit back-EMF of phase A at rated operation speed of 600 rpm acquired by the oscilloscope is shown in Fig. 29. The test result is consistent with FEA results.

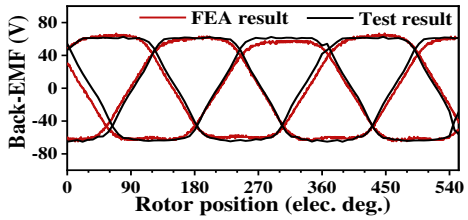

Fig. 29. Measured open-circuit back-EMF at 600 rpm.

By injecting rated current of 9A into the armature winding and testing the torque at different rotor position, the torque variation against current advance angle is shown in Fig. 30. The DPM-RM with slot PMs has higher torque than DPM-RM without slot PMs in all current angle. Also, with the special slot/pole combination, two machines have non-salient effect since three curves are all sinusoidal, which coincides with abovementioned inductance analysis. In addition, the test result of DPM-RM with slot PMs agrees well with simulation result.

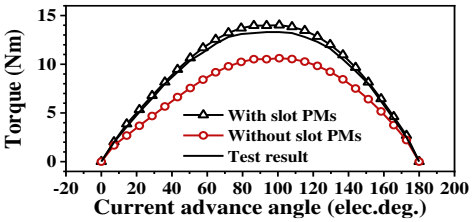

Fig. 30. Measured torque against current advance angle.

By injecting rated current of 9 A, the measured output steady torque, speed and phase currents acquired by the oscilloscope are denoted in Fig. 31. Fig. 31(a) shows the measured data under rated operation speed of 600 rpm, while Fig. 31(b) shows the measured date under high operation speed of 900 rpm. It is obvious that the output torque is about 13 Nm at 600 rpm and 9 Nm at 900 rpm due to flux weakening effect.

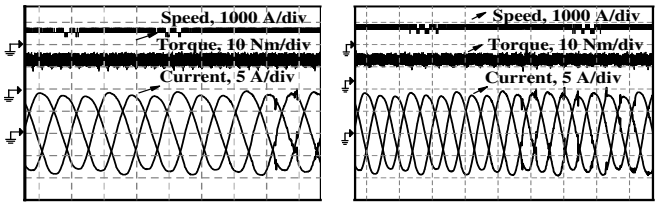

(a) (b)

Fig. 31. Measured output torque. (a) Rated speed of 600 rpm. (b) High speed of 900 rpm.

Under rated operation speed of 600 rpm, testing the torque at different armature excitation values, the torque against different copper loss is shown in Fig. 32(a) and the torque against different current density is denoted in Fig. 32(b). It can be seen that DPM-RM with slot PMs has higher torque than DPM-RM without slot PM in all copper loss and current density. Test result of DPM-RM with slot PMs agrees with simulation result.

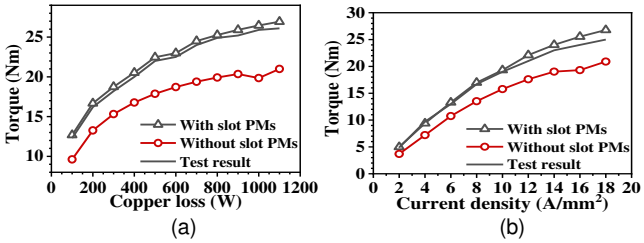

(a) (b)

Fig. 32. Torque variation. (a) Torque against copper loss. (b) Torque against current density.

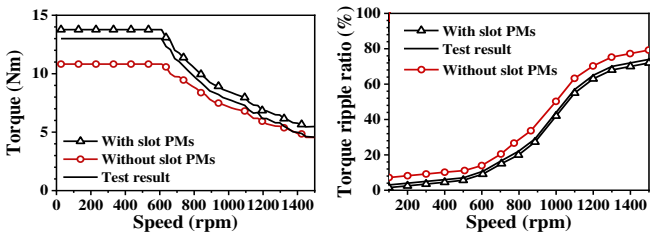

Fig. 33. Torque and torque ripple against speed. (a) Torque against speed. (b) Torque ripple against speed. (I_{rated}=9 A, U_{dc}=180 V).

Under rated current and limited DC voltage of 180 V, the torque and torque ripple are tested at different operation speed. It can be found that the DPM-RM with slot PMs has higher torque than DPM-RM without slot PMs in both constant torque region and constant power region as shown in Fig. 33(a). Meanwhile, the torque ripple increases along with the increase of speed. The DPM-RM with slot PMs has smaller torque ripple than DPM-RM without slot PMs in all speed range as denoted in Fig. 33(b). In addition, the test result of DPM-RM with slot PMs coincides with simulation result.

VI. Conclusion

This paper presents novel parallel-excited dual-PM reluctance machine (DPM-RM), which builds an integrated excitation field with both yoke PMs and slot PMs. Slot PMs is introduced to work with yoke PMs to enhance effective torque and stator core utilization factor. Through the flux analysis, with special slot/pole combination, DC component and even order harmonics of phase flux are eliminated, thus sinusoidal flux linkage and smooth torque can be attained. In addition, it is revealed in inductance analysis that the odd order harmonics of phase self-inductance are removed, resulting in small torque ripple with approximately constant phase self-inductance. A comparative study is performed between DPM-RM without slot PMs and with slot PMs. It can be concluded that the DPM-RM with slot PMs has the higher back-EMF, and higher torque than that without slot PMs. The open-circuit flux linkage, back-EMF, steady torque can be increased by 29.36%, 23.37%, and 27.26% through adopting slot PMs via FEA. The efficiency of DPM-RM with slot PMs is higher in both low-speed constant-torque and high-speed constant power region, which is suitable for application caring much about the energy saving. Furthermore, comparing with existing variable reluctance machine, the proposed DPM-RM has trapezoidal back-EMF, smaller self-inductance variation, smaller torque ripple. Due to the increased PM usage, the cost of machine may be higher than conventional double salient machines. To further reduce the machine cost, ferrite PM machine may be a solution and to improve the flux regulation capability, dc excitation-based hybrid design could be a potential solution.

References

[1] A. Kohara, K. Hirata and N. Niguchi, "Vibration Comparison of Current Superimposition Variable Flux Machine and Switched Reluctance Machine," 2018 XIII International Conference on Electrical Machines (ICEM), 2018, pp. 2337-2342.

[2] X. Sun, Z. Shi, G. Lei, Y. Guo, and J. Zhu, "Multiobjective design optim ization of an IPMSM based on multilevel strategy," *IEEE Trans. Ind. El ectron.*, vol. 68, no. 1, pp. 139-148, Jan. 2021.

[3] J. Bao, B. L. J. Gysen, K. Boynov, "Torque Ripple Reduction for 12-Stator/10-Rotor-Pole Variable Flux Reluctance Machines by Rotor Skewing or Rotor Teeth Non-Uniformity," IEEE Trans. Magn., vol. 53, no. 11, pp. 1-5, Nov. 2017.

[4] X. Sun, Z. Shi, and J. Zhu, "Multiobjective design optimization of an IP MSM for EVs based on fuzzy method and sequential Taguchi method," IEEE *Trans. Ind. Electron.,* vol. 68, no. 11, pp. 10592-10600, Nov. 2021.

[5] J. Bao, "Analysis of variable flux reluctance machines using hybrid analytical modelling," 2018 Thirteenth International Conference on Ecological Vehicles and Renewable Energies (EVER), 2018, pp. 1-7.

[6] M. M. Radulescu, "A new electronically-commutated doubly-salient permanent-magnet small motor," 1995 Seventh International Conference on Electrical Machines and Drives, 1995, pp. 213-216.

[7] G. Ming, L. Wu, "Comparative Study of Novel Doubly Fed Doubly Salient PM Machines with Different Stator/Rotor-Pole Number Combinations," *IEEE Trans. Magn.*, vol. 57, no. 6, pp. 1-5, June 2021.

[8] Y. Liao and T. A. Lipo, "Sizing and optimal design of doubly salient permanent magnet motors," 1993 Sixth International Conference on Electrical Machines and Drives (Conf. Publ. No. 376), 1993, pp. 452-456.

[9] B. Sarlioglu, Yifan Zhao and T. A. Lipo, "A novel doubly salient single-phase permanent magnet generator," Proceedings of 1994 IEEE Industry Applications Society Annual Meeting, 1994, pp. 9-15 vol.1.

[10] X. Zhu and M. Cheng, "A novel stator hybrid excited doubly salient permanent magnet brushless machine for electric vehicles," International Conference on Electrical Machines and Systems, 2005, pp. 412-415 Vol.1.

[11] G. Ming, L. Wu, "Comparative Study of Novel Doubly Fed Doubly Salient PM Machines with Different Stator/Rotor-Pole Number Combinations," *IEEE Trans. Magn.*, vol. 57, no. 6, pp. 1-5, June 2021.

[12] L. Wu, G. Ming, L. Zhang and Y. Fang, "Comparative Study Between Doubly Salient PM Machine with New Stator/Rotor-Pole Number Combination and Biased Flux PM Machine," 2019 IEEE International Electric Machines & Drives Conference (IEMDC), 2019, pp. 2174-2179.

[13] K. T. Chau, Q. Sun, Y. Fan, and M. Cheng, "Torque ripple minimization of doubly salient permanent magnet motors," *IEEE Trans. Energy Convers.*, vol. 20, no. 2, pp.352-358, Jun. 2005.

[14] Y. Gong, K. T. Chau, J. Z. Jiang, C. Yu, and W. Li, "Design of doubly salient permanent magnet motors with minimum torque ripple," *IEEE Trans. Magn.*, vol. 45, no. 10, pp. 4704-4707, Oct. 2009.

[15] W. Cui, "Optimized doubly salient memory motors with symmetric features using transposition design methods," International Conference on Power Engineering, Energy and Electrical Drives, 2011, pp. 1-7.

[16] X. Zhao, S. Niu, W Fu, "A novel Vernier reluctance machine excited by slot PMs and zero-sequence current for electric vehicle," *IEEE Trans. Magn.*, vol. 55, no. 6, pp. 1-5, Jun. 2019.

[17] X. Zhao, S. Niu, "Design and optimization of a novel slot-PM-assisted variable flux reluctance generator for hybrid electric vehicles," *IEEE Trans. Energy Convers.*, vol. 33, no. 4, pp.2102-2111, Dec. 2018.

[18] I. A. A. Afinowi, "Hybrid-excited doubly salient synchronous machine with permanent magnets between adjacent salient stator poles," *IEEE Trans. Magn.*, vol. 51, no. 10, pp. 1-9, Oct. 2015.

[19] I. A. A. Afinowi, Z. Q. Zhu, Y. Guan, "A novel brushless AC doubly salient stator slot permanent magnet machine," *IEEE Trans. Energy Convers.*, vol. 31, no. 1, pp. 283-292, March. 2016.

[20] Z. Q. Zhu *et al.*, "Hybrid excited stator slot PM machines with overlapping windings," *2018 XIII International Conference on Electrical Machines (ICEM)*, Alexandroupoli, 2018, pp. 2185-2191.

[21] X. Zhao, S. Niu, X Zhang, et al. "Design of a new relieving-DC-saturation hybrid reluctance machine for fault-tolerant in-wheel direct drive," *IEEE Trans. Ind. Electron.*, no. 99, pp.1-1, Nov. 2019.

[22] X. Zhao, S. Niu, W Fu, "A new modular relieving-DC-saturation Vernier reluctance machine excited by zero-sequence current for electric vehicle," *IEEE Trans. Magn.*, vol. 55, no. 7, pp. 1-5, July. 2019.

[23] Y. Shen, Z. Zeng, Q Lu, "Investigation of a modular linear doubly salient machine with dual-PM in primary yoke and slot openings," *IEEE Trans. Magn.*, vol. 55, no. 6, pp. 1-6, June. 2019.

[24] Y. Shen, "Design and analysis of linear hybrid-excited slot permanent magnet machines," *IEEE Trans. Magn.*, vol. 54, issue. 11, Nov. 2018.

[25] X. Zhao, S. Niu, X. Zhang and W. Fu, "Flux-Modulated Relieving-DC-Saturation Hybrid Reluctance Machine with Synthetic Slot-PM Excitation for Electric Vehicle In-Wheel Propulsion," *IEEE Tran. Ind. Electron.*, vol. 68, no. 7, pp. 6075-6086, July 2021.

[26] C. Liu, "Comparison of Stator-Permanent-Magnet Brushless Machines," *IEEE Trans. Magn.*, vol. 44, no. 11, pp. 4405-4408, Nov. 2008.

Jifu Jiang received the B,Sc. degree in electrical engineering from Wuhan University of technology, China, in 2016, and the M.Sc degree from Huazhong University of Science and Technology, China, in 2019. She is currently working toward the Ph.D. degree with the Department of Electrical Engineering, Hong Kong Polytechnic University, Hong Kong. Her research interests include machine design and machine control for electric vehicles and wind power generation.

Shuangxia Niu (Senior Member, IEEE) received the B.Sc. and M.Sc. degrees in electrical engineering from the School of Electrical Engineering and Automation, Tianjin University, Tianjin, China, and the Ph.D. degree in electrical engineering from the Department of Electrical and Electronic Engineering, the university of Hong Kong, Hong Kong. Since 2009, she has been worked with the Hong Kong Polytechnic University, Kowloon, Hong Kong, where she is currently an Associate Professor with the Department of Electrical Engineering. She has authored or co-authored over 100 published journal articles. Her research interests include machine design, renewable energy conversion, and applied electromagnetics.

Xing Zhao (Member, IEEE) received the B.Eng. degree from Nanjing University of Aeronautics and Astronautics, China, in 2014, and the Ph.D. degree from The Hong Kong Polytechnic University, Hong Kong SAR, in 2020, both in Electrical Engineering. Between 2019 and Oct. 2021, he served as a Research Assistant Professor with the Department of Electrical Engineering, The Hong Kong Polytechnic University. From Jul. 2019 to Jan. 2020, he was a Visiting Scholar with the Center for Advanced Power Systems, Florida State University, Tallahassee, USA. Currently, he is a Lecturer in the Department of Electronic Engineering, University of York, UK. He has authored over 50 technical papers in the international journals and conferences. His research interests include advanced electrical machines and power electronics for electric vehicles and renewable energy systems.